Modern Physics Letters B
Vol. 28, No. 7 (2014) 1450053 (9 pages)

DOI: 10.1142/S0217984914500535

World Scientific
www.worldscientific.com

Study on band gap structure of Fibonacci quantum superlattices by using the transfer matrix method

V. Ferrando

Centro de Tecnologías Físicas, Universitat Politècnica de València, Camí de Vera s/n, València 46022, Spain
viferma1@upv.es

J. C. Castro-Palacio

Departement Chemie, Physikalische Chemie, Universität Basel, Klingelbergstrasse 80, Basel CH-4056, Switzerland
juancarlos.castropalacio@unibas.ch

B. Marí

Departamento de Física Aplicada-IDF, Universitat Politècnica de València, Camí de Vera s/n, València 46022, Spain
bmari@fis.upv.es

J. A. Monsoriu

Centro de Tecnologías Físicas, Universitat Politècnica de València, Camí de Vera s/n, València 46022, Spain
jmonsori@fis.upv.es

Received 14 November 2013
Accepted 2 February 2014
Published 20 February 2014

The scattering properties of particles in a one-dimensional Fibonacci sequence based potential have been analyzed by means of the Transfer Matrix Method. The electronic band gaps are examined comparatively with those obtained using the corresponding periodic potentials. The reflection coefficient shows self-similar properties for the Fibonacci superlattices. Moreover, by using the generalized Bragg's condition, the band gaps positions are derived from the golden mean involved in the design of the superlattice structure.

Keywords: Superlattices; Fibonacci; quantum potential.

1. Introduction

The latest advances in nanotechnology have made possible the construction of very thin layers of material, as thin as monoatomic. This fact opens the possibility for the construction of the "so called" quantum superlattices, which are microelectronic

devices composed of alternating layers of two semiconductors with different band gaps deposited over a substrate.[1–4] If the band gaps of the combined materials are different, the result is a rectangular potential well for the electrons (holes) in the conduction (valence) band. The thickness of each semiconductor layer is about 10–100 atoms (1–10 nm). This can be done by using techniques such as: molecular beam epitaxy or metalorganic chemical vapor deposition.[1,2]

Taking advantage of the possibility of alternating very thin layers, experimentalists have gone beyond periodic structures, such as those with fractal distribution of the different layers, which means fractal distribution of band gaps. An example of such a device is that formed by layers of gallium arsenide (GaAs) placed in between layers of aluminium gallium arsenide (Al_xGa_{1-x}-As), where the alloy composition x may vary between 0 and 0.4, such as those fabricated by Axel and Terauchi[5] using $x = 0.3$ and a thickness of 0.28 nm for monolayers of Al_xGa_{1-x}-As. Another typical device has been fabricated with amorphous materials by alternating layers of amorphous germanium (a-Ge) and amorphous silicon (a-Si) deposited in a silicon substrate, as the fractal superlattices experimentally grown by Järrendahl *et al.*[6] in which each layer is thinner than 1.4 nm.

In order to be able to develop new designs of microelectronic devices for practical applications, theoretical and numerical physical modeling becomes an essential alternative.[6] In this context, quantum effects play a major role in determining the physical properties of these nanostructures. In the absence of an external electric field, semiconductor superlattices may be considered, in a first approximation, as quasi-one-dimensional systems of rectangular quantum wells separated by potential barriers (in the conduction band). When an external force is applied to the electrons in a quantum-well heterostructure, they do not respond as free particles due to the influence of other atoms. These effects may be taken into account by introducing an "effective mass" (m^*) which relates the particle motion to an external force (or potential) without worrying about all the atomic forces. Therefore, the scattering in semiconductor superlattices can be easily solved by means of the transfer matrix method (TMM) using an effective mass for the electrons.[7] The TMM has been extensively applied in different research areas (see for example, the recent studies of the Ising model by using the transfer matrix approach).[8,9] Within this context, in Refs. 11–13 authors have studied the scattering properties of fractal superlattices based on the Cantor set, by means of the numerical implementation of the TMM.

In line with our previous works, we consider in this paper, the study of another simple and interesting case, which is the scattering properties of particles by a quasi-periodic potential in the form of the Fibonacci sequence and the comparison with the corresponding periodic potential. The Fibonacci sequence is a highly motivating topic in science and technology. For instance, there are some situations in nature where this sequence can be seen.[14] In technology, a recent example of significant impact is the fabrication of quantum cascade lasers based on the Fibonacci sequence.[15]

The outline of this paper is the following. In Sec. 2, we formally present the problem, the features of the Fibonacci-based potential and the methodology followed by the solution of the problem. In Sec. 3, results and discussions are shown. We place special emphasis on the discussion of the self-similarity properties shown by the electronic band gaps, in comparison with the case of the equivalent periodic potential. Finally, in Sec. 4, some conclusions are drawn.

2. Presentation of the Problem

2.1. *Transfer matrix method*

The scattering of particles in one-dimensional potentials is driven by the time-independent Schrödinger equation:[16]

$$-\frac{\hbar^2}{2m}\frac{\partial^2\psi(x)}{\partial x^2} + V(x)\psi(x) = E\psi(x)\,, \tag{1}$$

where $\psi(x)$, m and E are the particle wave function, effective mass and energy, respectively; $\hbar$ is the Planck's constant and $V(x)$ is the quasi-periodic potential which can be represented by a piecewise constant function.

In Ref. 11, authors give details for the derivation of the reflection and transmission coefficients using general piecewise potentials. In order to help on the reading of this paper, we briefly recall here the most important aspects in this respect.

Let us consider the quantum scattering at the ith interface between two successive constant values of the piecewise potential, whose position, without loss of generality, has been taken as $x = 0$. Let ψ_i^+ and ψ_i^- be the forward and backward plane wave functions on the region where the potential value is V_i, so $\psi_i = \psi_i^+ + \psi_i^-$ there and

$$\psi_i^{\pm} = A_i^{\pm} e^{\pm i k_i x}\,, \qquad k_i = \frac{1}{\hbar}\sqrt{2m(E - V_i)}\,, \tag{2}$$

where $i = \sqrt{-1}$, k_i is the local particle momentum and $A_i^{\pm}$ are integration constants to be determined by applying the standard boundary conditions at the interface, the continuity of both the wave function and its derivative, i.e.,

$$\begin{aligned} &\psi_{i-1}(x=0) = \psi_i(x=0)\,, && A_{i-1}^+ + A_{i-1}^- = A_i^+ + A_i^-\,, \\ &\psi'_{i-1}(x=0) = \psi'_i(x=0)\,, && k_{i-1}A_{i-1}^+ - k_{i-1}A_{i-1}^- = k_i A_i^+ - k_i A_i^-\,, \end{aligned} \tag{3}$$

where the prime denotes differentiation. Equation (3) is a linear system of equations easily written in matrix notation as:

$$\begin{pmatrix} 1 & 1 \\ k_{i-1} & -k_{i-1} \end{pmatrix} \begin{pmatrix} A_{i-1}^+ \\ A_{i-1}^- \end{pmatrix} = \begin{pmatrix} 1 & 1 \\ k_i & -k_i \end{pmatrix} \begin{pmatrix} A_i^+ \\ A_i^- \end{pmatrix}\,, \tag{4}$$

and yielding

$$\begin{pmatrix} A_{i-1}^+ \\ A_{i-1}^- \end{pmatrix} = D_{i-1}^{-1} D_i \begin{pmatrix} A_i^+ \\ A_i^- \end{pmatrix}\,, \qquad D_i = \begin{pmatrix} 1 & 1 \\ k_i & -k_i \end{pmatrix}\,. \tag{5}$$

Hereon, the matrix $D_{i-1}^{-1}D_i$ is referred to as the wave scattering matrix.

After crossing the ith interface, the plane wave function propagates through the constant potential V_i until finding the next interface at a distance d_i. Let us write this wave function as

$$\tilde{\psi}_i^{\pm} = A_i^{\pm} e^{\pm ik_i d_i} e^{\pm ik_i x} = \tilde{A}_i^{\pm} e^{\pm ik_i x}\,, \tag{6}$$

and a wave propagation matrix P_i can be defined as

$$\begin{pmatrix} \tilde{A}_{i-1}^{+} \\ \tilde{A}_{i-1}^{-} \end{pmatrix} = \begin{pmatrix} e^{ik_i d_i} & 0 \\ 0 & e^{-ik_i d_i} \end{pmatrix} \begin{pmatrix} A_i^{+} \\ A_i^{-} \end{pmatrix} = P_i \begin{pmatrix} A_i^{+} \\ A_i^{-} \end{pmatrix}. \tag{7}$$

Both the scattering and propagation matrices can be used to solve the general problem of the scattering with a piecewise constant potential of N potential wells. The successive application of the scattering and propagation matrices yields,

$$\begin{pmatrix} A_0^{+} \\ A_0^{-} \end{pmatrix} = D_0^{-1} D_1 \begin{pmatrix} A_1^{+} \\ A_1^{-} \end{pmatrix} = D_0^{-1} D_1 P_1 D_1^{-1} D_2 \begin{pmatrix} A_2^{+} \\ A_2^{-} \end{pmatrix}, \tag{8}$$

and the most general form,

$$\begin{pmatrix} A_0^{+} \\ A_0^{-} \end{pmatrix} = M \begin{pmatrix} A_{N+1}^{+} \\ A_{N+1}^{-} \end{pmatrix}, \qquad M = D_0^{-1} \left(\prod_{i=1}^{N} D_i P_i D_i^{-1} \right) D_{N+1}\,. \tag{9}$$

Both the reflection and transmission coefficients of the scattering of a quantum particle, incoming from the left, with the N-well potential are determined by the coefficients of the matrix M,

$$\begin{pmatrix} A_0^{+} \\ A_0^{-} \end{pmatrix} = \begin{pmatrix} M_{11} & M_{12} \\ M_{21} & M_{22} \end{pmatrix} \begin{pmatrix} A_{N+1}^{+} \\ 0 \end{pmatrix}, \tag{10}$$

where no backward particle can be found on the right side of the potential, so $A_{N-1}^{+} = 0$ and N identifies the Nth well. In this respect, the reflection and transmission coefficients are expressed as,

$$R = \frac{|A_0^{-}|^2}{|A_0^{+}|^2} = \frac{|M_{21}|^2}{|M_{11}|^2}\,. \tag{11}$$

2.2. *Fibonacci sequence based potentials*

Let us now consider a system whose well distribution follows a Fibonacci sequence. The Fibonacci numbers, F_i with $i = 0, 1, 2, \ldots$, are characterized by the relation $F_{i+1} = F_i + F_{i-1}$, with $F_0 = 0$ and $F_1 = 1$, so $F = \{0, 1, 1, 2, 3, 5, 8, 13, 21, \ldots\}$. In a similar way, we have considered the Fibonacci sequence based on a recursive relation, $D_{i+1} = \{D_i, D_{i-1}\}$ for $i \geq 1$, with $D_0 = \{B\}$, $D_1 = \{A\}$, $D_2 = \{AB\}$, $D_3 = \{ABA\}$, $D_4 = \{ABAAB\}$, $D_5 = \{ABAABABA\}$ and so on. It can be noticed that the sequence at the stage S, D_S, will have F_{S+1} elements distributed in F_S times "A" and F_{S-1} times "B" so that $F_{S+1} = F_S + F_{S-1}$. This sequence

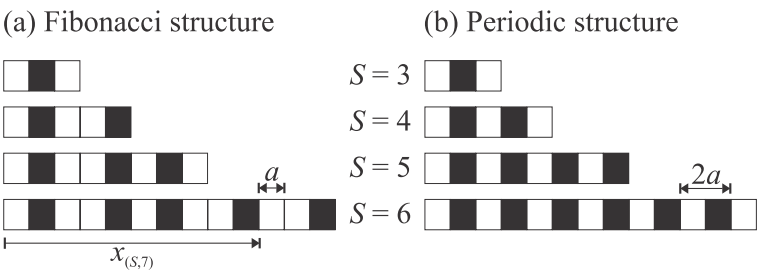

Fig. 1. Diagrams of the well distributions of the potential for (a) a Fibonacci sequence for several values of S and (b) its associated periodic distribution. In this representation, open and filled segments correspond to the values $-V$ and 0, respectively, of the well distribution.

has been previously employed in the design of diffractive lenses,[17] between other applications. In our case, A and B define the well distribution of the potential whose values are $-V$ and 0, respectively.

Hence, the number of wells A (of depth $-V$) for the order S, will be F_S, separated by F_{S-1} gaps. The width of the well has been called "a". The distance between wells (filled segments) is also "a" in our simulations. This fact makes the calculation easier for the model still general. In Fig. 1, the diagrams of the well distributions for the Fibonacci sequence (panel a) and its associated periodic potential (panel b) have been shown. A and B are represented by open and filled segments, respectively.

In Fig. 1, $x_{(S,i)}$ with $i = 1, 2, \ldots, F_S$ represents the left position of the Fibonacci sequence of the ith well. Mathematically, this parameter can be obtained as $x_{(S,i)} = (\lfloor \tau i \rfloor - 1)a$, where the symbol $\lfloor\ \rfloor$ represents the floor function, which denotes the largest integer less than or equal to the argument. The parameter τ is called the golden mean or magic number and it is obtained as:

$$\tau = \lim_{S\to\infty} \frac{F_S}{F_{S-1}} = \frac{1+\sqrt{5}}{2} \approx 1.618\,, \tag{12}$$

which is the ratio between the number of quantum wells (F_S) and the number of gaps (F_{S-1}) for large generating orders (S). In a similar way, we consider the associated periodic distribution with period $2a$. The Fibonacci case can be understood as a conventional periodic distribution where the position of some wells of the potential has been interchanged.

Using the TMM, the reflection coefficient, R, for several values of S as a function of the particle energy (horizontal axis) and the depth of the wells (vertical axis), has been determined. According to Eq. (11), the reflection coefficient, R, can be obtained from the coefficients of the transfer matrix, M. The matrix, M, has 2×2 terms obtained iteratively using Eq. (9) which involves the wave scattering matrices, D [Eq. (8)] in the wave propagation matrices [Eq. (7)]. For example, in the simple case of $S = 3$, two wells separated by a gap are present. To model this situation, four scattering matrices, D (one for each interface) and three propagation matrices,

P (two potential wells and a gap between them) are needed. In order to reduce the difficulty of the calculations, non-dimensional normalized variables are preferably used. The energy E and the potential V have been normalized by the length of the segment a according to:

$$\phi = \frac{\sqrt{2mE}}{\hbar}a\,, \qquad \phi_V = \frac{\sqrt{2mV}}{\hbar}a\,. \tag{13}$$

By using this normalization, the phase shifts of the wave functions involved in the propagation matrices [Eq. (7)] are reduced to ϕ for the regions of the gaps and to $\sqrt{\phi^2 + \phi_V^2} = \frac{1}{\hbar}\sqrt{2m(E+V)}a$ for the regions of the quantum wells.

3. Results and Discussions

In Fig. 2(a), the plot of the normalized energy (ϕ) *versus* the order S is shown for the case of the equivalent periodic structure. The period of the structure of order S can be represented by $F_{S+1}/2$. For example, for $S = 12$, we have $F_{13}/2 = 233/2 = 116.5$ periods. It can be noticed that the band gap gets more defined as S increases. Although higher orders of the Fibonacci sequence have been simulated, we only show the reflection spectra up to $S = 12$ in Fig. 2 for simplicity. It can be noticed in Fig. 2 that a gray-code bar represents the exact value of the reflection coefficient, R, different from works published previously, which only show the regions of the bands with a binary code.[18]

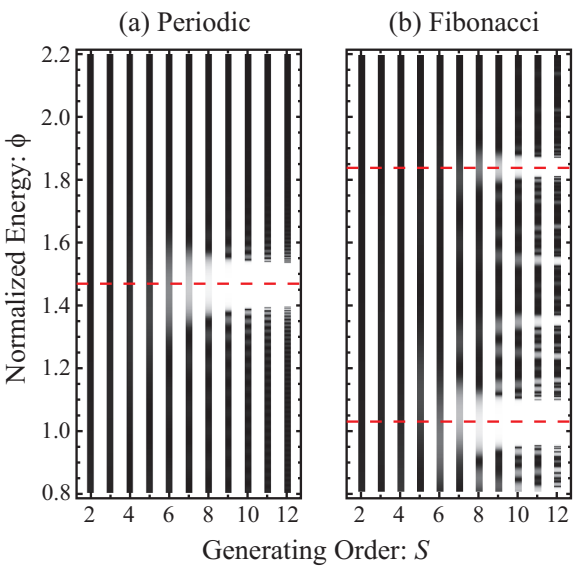

Fig. 2. Values of the normalized energy (ϕ) *versus* the order S. In panel (a) the case for the periodic structure is shown and in panel (b) the Fibonacci sequence based structure. The gray-code bar represents the reflection coefficient, R, of these structures, being $R = 1$ in the white regions and $R = 0$ in the black ones.

According to the well-known Bragg's law, the reflection coefficient R, is maximum when the phase shift between the incident and reflected waves at the different quantum wells is an integer number (n) times 2π. This condition can be expressed in terms of ϕ and ϕ_V as,

$$\sqrt{\phi_n^2 + \phi_V^2} + \phi_n = n\pi\,. \tag{14}$$

For $n = 1$ and $\phi_V = 0.8$ in our calculations, we obtain, $\phi_1 = 1.469$. This value corresponds to the position of the dashed line in Fig. 2(a).

The case of the Fibonacci structure is shown in Fig. 2(b). As observed for the periodic case, the bands get more defined as S increases. Besides, multiple secondary bands with a fractal response appear as a consequence of the self-similar distribution of the Fibonacci sequence. These highly fragmented band structures can find applications in the field of photovoltaics or as efficient electronic filters (see Refs. 19, 20 and those cited within, for more details about superlattices applications). The values of energy of the centre of the band gaps of the main bands can be derived from the generalized Bragg's condition:

$$\tau\sqrt{\phi_{p,q}^2 + \phi_V^2} + \phi_{p,q} = \pi(p + q\tau)\,, \tag{15}$$

where p and q are integer numbers.

It can be noticed that Eq. (15) becomes Eq. (14), for $\tau = 1$. This is because τ represents the ratio between the number of wells and gaps, which are equal for the periodic case. In the Fibonacci superlattice, for $p = 1$ and $q = 0$ [lower dashed line in Fig. 2(b)], we get $\phi_{1,0} = 1.031$ and for $p = 0$ and $q = 1$ [upper dashed line in Fig. 2(b)], we get $\phi_{0,1} = 1.839$. It can be observed that the calculated values are in good agreement with the positions of the band gap centers in the figure. Analogous results have been obtained in Ref. 21 for optical Fibonacci multilayers.

In order to show the self-similar behavior of the reflection coefficient obtained with the Fibonacci superlattice, in Fig. 3 the results for $S = 7, 8$, and 9 are shown. It can be noticed that a wide peak at the stage S is replaced by two narrower and higher peaks at the stage $S + 1$. Therefore, the reflection coefficient at each higher state is a modulated version of that associated to the previous one.

In the following, we will analyze the behavior of the obtained band gaps as a function of the depth of the wells. In Fig. 4(a), the plot of the normalized energy (ϕ) *versus* the normalized potential (ϕ_V) is shown for the case of the periodic structure. The calculations have been done for $S = 10$. In order to evaluate the effect of the well depth, the Bragg's condition [Eq. (14)] is used. For weak particle–structure interactions, the well depth tends to zero ($V \to 0$), that is, $\phi_V \to 0$ then, the band widths decrease and the positions of the normalized energy Bragg's peaks tend to $\phi_n = n\pi/2$. For $n = 1$, the value of $\phi_1 = \pi/2$ can be noticed on the y-axis of the plot. On the contrary, as the well depth (V) increases (strong interactions), that is, ϕ_V increases; the values of ϕ_1 decrease. This fact is derived from Eq. (14) and can be observed in Fig. 4. In the case of the band gap width, it decreases as the values of ϕ_V decrease.

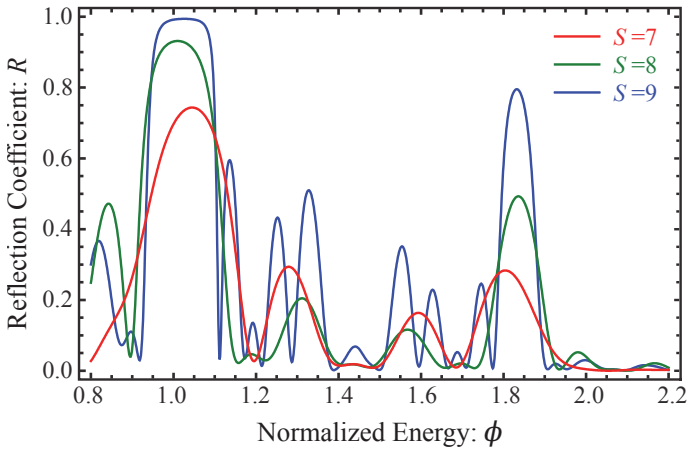

Fig. 3. (Color online) Reflection coefficient (R) *versus* the normalized energy (ϕ) for the Fibonacci structure. Results for $S = 7$, 8 and 9 are shown. These results have also been included in Fig. 2(b) as gray-code bars.

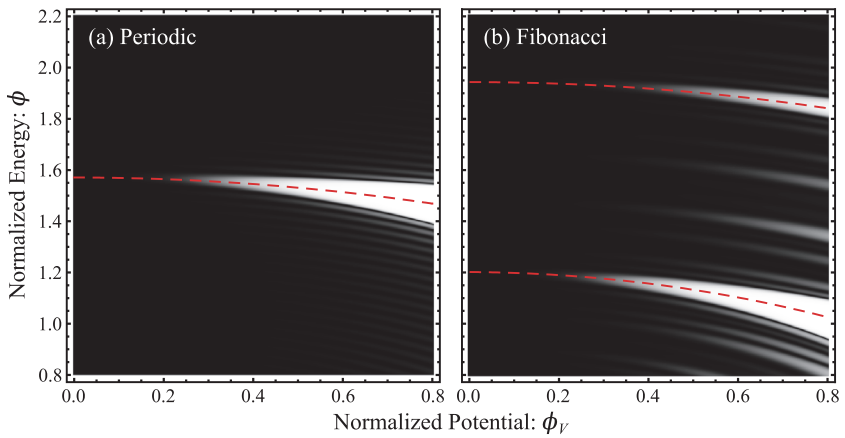

Fig. 4. (Color online) Values of the normalized energy (ϕ) *versus* the normalized potential (ϕ_V). In panel (a), the case for the periodic structure is shown and in panel (b), the Fibonacci sequence based structure is shown. The figure illustrates the results for the order $S = 10$. The dashed red line indicates the Bragg's condition.

In Fig. 4(b), the case of the Fibonacci sequence structure is represented. By using the generalized Bragg's condition of Eq. (15), the band gaps can be characterized. For $\phi_V \ll \phi$ (weak interactions) and $p = 1$, $q = 0$, from Eq. (15), we get $\phi_{1,0} = \pi/\tau^2 = 0.4197$ and for $p = 0$ and $q = 1$, we get $\phi_{0,1} = \pi/\tau = 1.1482$. A further relationship between the band gap center positions can be derived from the golden mean, that is, $\phi_{1,0}/\phi_{0,1} = \tau$, which is related to the mathematical properties of the Fibonacci sequence considered in the design of the superlattice structure.

4. Conclusions

In this paper, the TMM has been used to obtain the reflection coefficient spectrum in aperiodic quantum superlattices based on a one-dimensional Fibonacci sequence like potential. Results have been explained comparatively to the case, when an equivalent finite periodic potential is used. Fibonacci superlattices also yield electronic band gaps which exhibit a self-similar behavior. The positions of the band peaks have been found to be related to the golden mean. This work also suggests the use of the matrix transfer method to treat other interesting proposals of one-dimensional aperiodic sequences such as Thue Morse, Period-doubling and Silver mean.

Acknowledgments

We acknowledge the financial support from Ministerio de Ciencia e Innovación (grant FIS2011-23175), and Generalitat Valenciana (grant PROMETEO2009-077), Spain.

References

1. B. R. Nag, *Physics of Quantum Well Devices* (Kluver Academic, Dordrecht, 2001), p. 312.
2. P. Roblin, *High-Speed Heteroestructure Devices: From Device Concepts to Circuit Modeling* (Cambridge University Press, New York, 2002), p. 688.
3. R. M. Kolbas and N. Holonyak, *Am. J. Phys.* **52** (1984) 431.
4. R. Mazurczyk, *Chaos, Solitons & Fractals* **10** (1999) 1971.
5. F. Axel and H. Terauchi, *Phys. Rev. Lett.* **66** (1991) 2223.
6. K. Järrendahl, M. Dulea, J. Birch and J.-E. Sundgren, *Phys. Rev. B* **51** (1995) 7621.
7. L. L. Sanchez-Soto, J. J. Monzón, A. G. Barriuso, J. F. Cariena, *Phys. Rep.* **513** (2012) 191.
8. T. Kaya, *Int. J. Mod. Phys. B* **26** (2012) 1250085.
9. T. Kaya, *Mod. Phys. Lett. B* **26** (2012) 1250111.
10. J. A. Monsoriu, F. R. Villatoro, M. J. Marín, J. Pérez and Ll. Monreal, *Am. J. Phys.* **74** (2006) 831.
11. J. A. Monsoriu, F. R. Villatoro, M. J. Marín, J. F. Urchueguía and P. F. Fernández de Córdoba, *Eur. J. Phys.* **26** (2005) 603.
12. F. R. Villatoro and J. A. Monsoriu, *Phys. Lett. A* **372** (2008) 3801.
13. J. C. Castro-Palacio, F. R. Villatoro, O. Mendoza-Yero, L. Velazquez-Abad and J. A. Monsoriu, *Fractals* **20** (2012) 89.
14. A. J. Fleming, *Nature* **418** (2002) 723.
15. L. Mahler, A. Tredicucci, F. Beltram, C. Walther, J. Faist, H. E. Beere, D. A. Ritchie and D. S. Wiersma, *Nat. Photonics* **4** (2010) 165.
16. N. W. Ashcroft and N. D. Mermin, *Solid State Physics* (Saunders, Philadelphia, 1976), p. 848.
17. A. Calatayud, V. Ferrando, L. Remón, W. D. Furlan and J. A. Monsoriu, *Opt. Express* **21** (2013) 10234.
18. E. L. Albuquerque and M. G. Cottam, *Phys. Rep.* **376** (2003) 225.
19. E. Maciá, *Rep. Prog. Phys.* **75** (2012) 036502.
20. E. Maciá, *Rep. Prog. Phys.* **69** (2006) 397.
21. W. J. Hsueh, C. H. Chang, Y. H. Cheng and S. J. Wun, *Opt. Express* **20** (2012) 26618.